JACS
JOURNAL OF THE AMERICAN CHEMICAL SOCIETY
pubs.acs.org/JACS
Article

Interaction-Dependent Secondary Structure of Peptides in Biomolecular Condensates

Keegan A. Lorenz-Ochoa, Moonyeon Cho, Sapun H. Parekh, and Carlos R. Baiz*

Cite This: J. Am. Chem. Soc. 2024, 146, 33616−33625
Read Online
ACCESS | Metrics & More | Article Recommendations | Supporting Information

ABSTRACT: Biomolecular condensates provide a mechanism for compartmentalization of biomolecules in eukaryotic cells. These liquid-like condensates are formed via liquid−liquid phase separation, by a plethora of interactions, and can mediate several biological processes in healthy cells. Expansions of dipeptide repeat proteins, DPRs, in which arginine rich DPRs like poly-proline-arginine (PR), and poly-glycine-arginine (GR), partition RNA into condensates can however induce cell toxicity. Here, we use $(GR)_{20}$ as a model for biological poly-GR and condense it using either excluded volume interactions with polyethylene glycol (PEG) as a crowder or direct electrostatic interactions with RNA oligomers. Using two-dimensional infrared (2D IR) spectroscopy, we observe that $(GR)_{20}$ condensed through an excluded volume forms β-sheet structures, whereas $(GR)_{20}$ condensed with RNA forms loops. We also investigate local hydrogen-bond dynamics in the condensate and compare the measurements with molecular dynamics simulations. Hydrogen bond lifetimes undergo a marked slowdown compared to dynamics in the dilute phase. This is representative of confined water within the percolated networks inside the condensate due to the interaction present in the condensate disrupting H-bond networks. Overall, our results show that both protein structure and dynamics are inherently dependent on the type of interactions that stabilize the condensates.

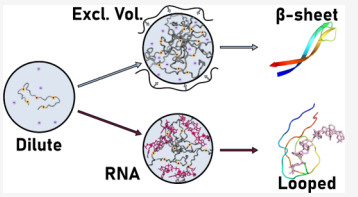

INTRODUCTION

Biomolecular condensates provide a mechanism to impart spatiotemporal control over biochemical processes in the cell.[1] Self-assembled via liquid−liquid phase separation, condensates can be described as dense nanometer-scale droplets containing primarily proteins and nucleic acids.[2−5] Due to the lack of an impermeable barrier, biomolecular condensates, BMCs, have a uniquely dynamic environment wherein biomolecules can rapidly exchange with the cytosol.[6−8] The balance of complex interactions result in the formation of nanometer-scale percolated networks within the droplets.[9−12] The driving forces involve a combination of direct biomolecule interactions including electrostatic forces, cation-π, and π stacking; in addition to hydrogen-bonding.[4,12−15] Water molecules mediate many of these key interactions, and characterizing the complex balance of these interactions and the local solvation environments is critical to understanding the fundamental forces that dictate the local morphologies, stabilities, and dynamics of biomolecular assemblies.[16−18]

Phase separating proteins often contain low-complexity domains, in addition to arginine-rich dipeptide repeats (DPRs), exhibiting high phase-separation propensities.[19−22] DPRs are the result of expansion mutations in the C9orf72 gene which produces several different sequences although arginine-rich sequences such as poly-GR, glycine-arginine, and poly-PR, proline-arginine, are particularly cytotoxic.[23−28] This arginine-rich sequence phase separates in a variety of conditions; however, to our knowledge, their microscopic structure, and local environments have not been characterized.[24,29] Poly-GR and poly-PR phase separate under a variety of environments: under the influence of a crowder, such as polyethylene glycol (PEG), through electrostatic interactions with RNA oligomers, or by crowding with other biomolecules.[29−31] Considering the flexibility of the peptide backbone as well as the complex nature interactions that lead to phase separation, it is important to uncover the role of the environment on the residual secondary structure of the peptide.[32−34] Many BMC studies are carried out with artificial crowders, such as polyethylene glycol (PEG), but in vivo condensates contain a range of biomolecules including RNA. Therefore, characterizing the structure and dynamics of BMCs formed under different conditions is fundamental to evaluating the complex forces that stabilize the condensates and uncovering the underlying *in vitro* versus *in vivo* differences.

Much of the focus on BMCs has been on understanding thermodynamic conditions that stabilize assemblies, but little is known about the secondary structure of proteins in the droplets because measuring secondary structure remains a challenging when using conventional biophysical techniques.[29,35−38] Two-dimensional infrared (2D IR) spectroscopy, in the amide I region (backbone carbonyl stretches) can directly access secondary structures of proteins in a variety of

Received: August 15, 2024
Revised: November 15, 2024
Accepted: November 18, 2024
Published: November 26, 2024

https://doi.org/10.1021/jacs.4c11226
J. Am. Chem. Soc. 2024, 146, 33616−33625

environments.[32,39−44] Additionally, as an ultrafast technique, 2D IR measures molecular motions on the picosecond time scale, yielding a local view of the dynamic environments within the condensate.[16,18,45,46] Using 2D IR spectroscopy on a model DPR, $(GR)_{20}$, prepared through either crowding with PEG, or by electrostatic interactions with an RNA oligomer, we are able to characterize the differences in residual secondary structure as well as changes in the local environment around the peptide (Figure 1).

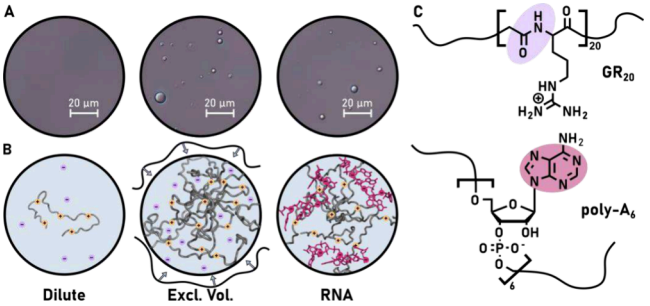

Figure 1. (A) Phase-contrast images of 500 μM $(GR)_{20}$ in dilute phosphate buffer, 30 volume% PEG (Excl. Vol.), and 2 mg/mL poly-A for a charge ratio of 1.97 $(GR)_{20}$:poly-A. (B) Schematic illustration of $(GR)_{20}$ peptides, in gray with positive charges from the arginine, subjected to dilute phosphate buffer, purple ions, 30% PEG and 2 mg/mL of poly-A with PEG shown on the outside as a crowder and poly-A shown in pink with pink ions representing the negatively charged phosphate backbone. (C) Molecular structures of $(GR)_{20}$ and poly-A.

RESULTS AND DISCUSSION

2D IR of $(GR)_{20}$ Peptides in Different Environments. Microscope images of $(GR)_{20}$ show approximately 3 μm diameter droplets, confirming phase separation under the experimental conditions used for spectroscopy (Figure 1A). Diameter distribution histograms for both types of condensates are included in Figure S2. Measured 2D IR spectra in the 1620−1680 cm^{-1} amide I region of the spectrum, consist primarily of carbonyl stretches. These 2D IR lineshapes report on the secondary structure of the peptide backbone.[45,47,48] Additionally, the evolution of lineshapes with waiting time report on the dynamics of the local environments around the peptide backbone.[49] Three different samples were studied (Figure 1B): 1. Dilute $(GR)_{20}$ consisting of the peptide in a buffer solution, which does not undergo liquid−liquid phase separation, this sample serves to measure the "bulk" dynamics when the peptide backbone is fully exposed to water; 2. $(GR)_{20}$ in a buffer solution with 30 volume% PEG as a crowding agent to induce droplet formation, and 3. $(GR)_{20}$ with RNA (poly-A) that undergoes liquid−liquid phase separation as a result of strong electrostatic interactions between the positively charged peptide side-chains and the negatively charged RNA backbone. Poly-A was used due to the relatively simple infrared features that can be readily subtracted from the amide region; furthermore, other RNA sequences and structures would require more advanced subtraction techniques to isolate the contribution from the protein amide band.[29,50] The high concentration of PEG is to maintain comparable conditions to previous studies with similar systems to $(GR)_{20}$.[22,32] There is evidence to show that in similar systems, PEG interactions do not dominate over protein−protein interactions and that PEG, in addition to crowding through excluded volume effects, modulates the hydrogen bonding environment further altering stability of proteins within the crowded environment.[51−53] The general features of proteins that determine favorable PEG-protein interaction is poorly understood and is worth future studies; however, while PEG may interact with the peptide in the condensate phase, direct interactions likely do not dominate over peptide−peptide interactions, thus it is expected that PEG behaves primarily a crowding agent.[45,51,54]

Spectra of the three $(GR)_{20}$ samples (Figure 2) exhibit a positive peak elongated along the diagonal centered around

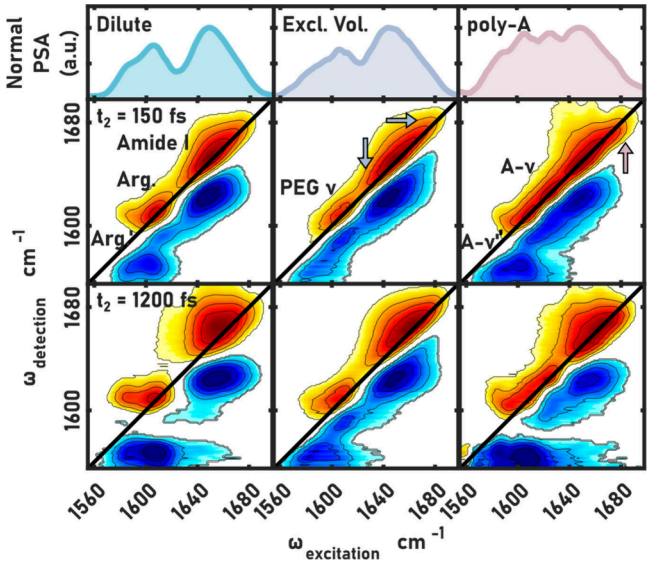

Figure 2. Experimental 2D IR spectra of $(GR)_{20}$ in dilute buffer, 30% PEG, and 2 mg/mL of poly-A along with PSAs of each spectra on top to highlight changes in lineshapes between each system. Spectra were measured at a waiting time of 150 fs. For clarity, noise below 20% of the maximum is cut off. Differences in line shape are highlighted with arrows. The structure of $(GR)_{20}$ in PEG seems to exhibit higher intensities near the edges of the amide I band. The structure of $(GR)_{20}$ in poly-A shows a distinct feature in the higher frequency region.

1650 cm^{-1} associated with the random coil like disordered structure of $(GR)_{20}$ and labeled amide I arising from the broad distribution of structures associated in addition to the H-bonding environments of $(GR)_{20}$.[55] Additionally, the spectra contain two low-frequency diagonal peaks centered around 1608 and 1584 cm^{-1} labeled Arg and Arg', respectively. These correspond to the arginine side chains C═N symmetric and asymmetric stretching modes from the guanidinium group.[56,57] Off diagonal features in the spectra are also attributed to intramolecular coupling of the two arginine peaks and grow with increasing waiting time delay (Figure 2).[56] Upon phase separation induced by PEG, the amide band center shifts from 1650 to 1644 cm^{-1} and contains the same lower frequency diagonal peaks assigned to the arginine side chains. However, in these spectra, these peaks are overlapped with a peak centered around 1605 cm^{-1} associated with an overtone of the PEG CH_2 wagging mode. This is a strong band due to the high concentration of PEG in the sample. Additionally, this spectrum also contains higher intensities in the lower and higher frequency regions, as indicated by the blue arrows in Figure 2. Upon phase separation with poly-A, the amide band remains centered near 1650 cm^{-1} showing only a slight 2 cm^{-1}

https://doi.org/10.1021/jacs.4c11226
J. Am. Chem. Soc. 2024, 146, 33616−33625

shift to ~1648 cm^{-1} similar to the dilute phase, representative of a largely disordered structure inside the condensate phase in addition to a similar H-bonding environment as in the dilute phase. Despite the amide band remaining centered around 1647 cm^{-1} the band has a new distinct feature arising around 1674 cm^{-1} (pink vertical arrow). In addition to this new feature in the amide band, there are two more diagonal features centered around 1624 and 1572 cm^{-1} representative of the poly-A adenosine ring modes labeled A-ν and A-ν' respectively.[50] Moreover, the ring mode at 1624 cm^{-1} in the condensate phase is notably shifted from the ring mode in the dilute phase centered around 1629 cm^{-1}, shown in Figure S6. likely a result of the cation-pi interaction with the poly$(GR)_{20}$ arginine side chains. Due to overlapping cross peaks from the arginine side chain and ring mode coupling, any possible vibrational coupling between the arginine side chain and the adenine moiety may be difficult to uncover.

The differences between spectra in Figure 2, can be more clearly observed by subtracting the dilute spectrum features from both the PEG and poly-A spectra; the resulting difference spectra are shown in Figure 3A. In the PEG sample, two distinct positive features are centered around 1633 and 1682 cm^{-1}. To quantify changes in secondary structure induced by phase separation through crowding with PEG or electrostatic interactions by poly-A, we analyzed one-dimensional pump-slice amplitude (PSA) spectra extracted from each 2D IR spectrum. Briefly, PSA analysis involves computing the difference between the minimum and maximum amplitudes at each excitation frequency.[58] The resultant spectrum can be interpreted similarly to an FTIR but with higher sensitivity to subpopulation changes. PSA spectra benefit from a combination of background suppression and nonlinear signal scaling of 2D IR.[58,59] PSA has previously been used to extract peptide structure in solution.[60,61] The PSA spectra were then analyzed by band fitting as described in Section S3.[62,63] In brief, populations of each secondary structure are calculated as a ratio of the different Gaussians to the cumulative area of the amide I band. Final Gaussian peaks were computed as an average of one-hundred independent fits with random starting points for peak positions, amplitudes, and widths (Figure 3B–C) with the uncertainties included in Section S3. The results show a marked decrease in random coil content in either the PEG or poly-A condensates compared to dilute $(GR)_{20}$. These results indicate that the peptide becomes more structured in the condensate phase. Interestingly, PEG tends to have a higher population, 28% of the amide area β-sheet modes labeled as β–$\nu_{\perp}$. This lower frequency mode is associated with coupling across different sheet strands and has a higher population compared to the poly-A condesnate spectrum with only 18% of the amide I band area attributed to β–$\nu_{\perp}$.[41,64,65] This difference in populations attributed to a difference in secondary structure. Additionaly, there is a small increase in the higher frequency populations attributed to the loop and β–$\nu_{\parallel}$ bands. Previous studies had shown that these peaks exhibited by the difference spectra could be attributed to various poly proline structures; however, the system of interest is another alternate DPR, $(PR)_{20}$. The high concentration of proline in $(PR)_{20}$ could prevent structures involving hydrogen bonding like the aforementioned β-sheet we believe is present in $(GR)_{20}$.[32] To further validate the interpretation of the observed spectral differences based on predicted structures, we performed structure-based spectral simulations on high-confidence structures produced by AlphaFold 3 of a single

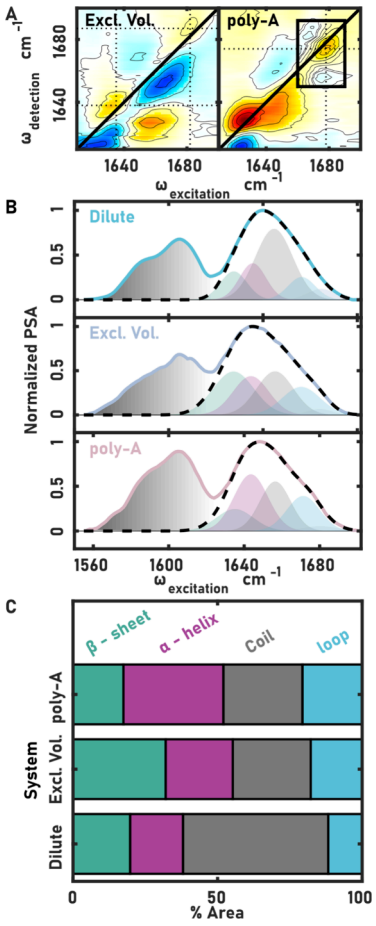

Figure 3. (A) Difference spectra of $(GR)_{20}$ in the condensate phase of both Excl. Vol. and poly-A. In both cases, the features of GR_{20} in the dilute phase subtracted out each at t_2 = 150 fs. Distinct peaks emerge along the diagonal in the case of Excl. Vol. intensity emerges around 1633 and 1676 cm^{-1}, respectively. A distinct peak around 1676 cm^{-1} emerges upon phase separation with poly-A. (B) Fitting results shown under the amide. Gaussians correspond to the different secondary structures. The poly-A spectra have the nucleotide ring mode subtracted for clarity. (C) Fitting results highlighting the percentage population of the different secondary structures. Error is produced by the upper and lower bounds of the fitting results and shown in Section S3.

$(GR)_{20}$ peptide as well as a $(GR)_{20}$ interacting with a single poly-A RNA oligomer (Section S4).[55] While the peptides are disordered, and the conformational ensemble may cannot be represented by any single structure, AlphaFold3[66] structures give some confidence that $(GR)_{20}$ has high β-sheet formation propensity while the $(GR)_{20}$ poly-A structure shows a primarily looped structure surrounding the poly-A strand likely a result of favorable elecrostatic interations between the poly-A and $(GR)_{20}$. Generally, these simulations are consistent with the fittiing results that indicate more β-sheet prevalence in the PEG condensate while the condensate formed with poly-A is a looped structure with a strong high-frequency peak.

Dynamics of GR_{20} in the Dilute and Condensate Phases. To investigate the picosecond dynamics of the amide backbone, center line slope analysis (CLS) was performed on the amide I band of the peptide in the dilute and condensate phases. In short, this analysis reports on frequency fluctuations of the vibrational probe as a result of the local environment (Figure 4A, Section S5).[67−69] Moreover, while the amide band

https://doi.org/10.1021/jacs.4c11226
J. Am. Chem. Soc. 2024, 146, 33616−33625

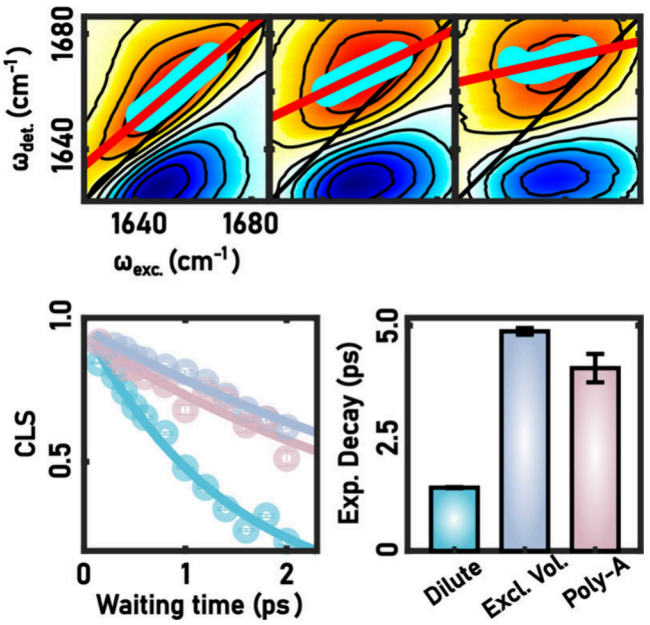

Figure 4. (A) Example center-line-slope analysis for GR_{20} in the dilute phase. Blue circles are the selected frequencies that are used for the fit indicated by the red line. (B) Fitting results for the experimental dynamics. The parameters extracted from the CLS analysis are tabulated in Section S5.

is delocalized across peptide backbones, previous studies show that despite delocalized vibrations, reported dynamics are largely a result of local environment fluctuations.[70−72] The CLS decay (Figure 4B) is fit to an monoexponential decay and the lifetime is shown in (Figure 4C). A marked slowdown in dynamics is observed in the condensate phases compared to the dilute phase. The CLS decay constant is 1.40 ps for the dilute phase, compared to 4.87 and 4.06 ps for the Excl. Vol. (PEG) and RNA condensates respectively, though the 2 ps waiting-time measurement window, limited by the vibrational lifetime, does not allow for accurate determination of longer decay times in the condensate phase. Similar slowing of dynamics have been reported for other peptides in the condensate phase, and has been attributed to trapped water resulting in slower hydrogen bond dynamics in the condensate.[16,18] To gain insight into these differences in the dynamics and a more atomistic interpretation, MD simulations were performed on $(GR)_{20}$ subjected to each of the different conditions.

Hydrogen-Bonding dynamics from MD Simulations. Molecular dynamics (MD) simulations provide a molecular description of the dilute and condensate environments allowing for the extraction of H-bond populations and H-bond dynamics which can be directly compared with experimental measurements. Here we constructed three systems: 1. A "dilute" peptide system consisting of a single $(GR)_{20}$ peptide in the simulation box; 2. An "excluded volume" system which consists of ten randomly packed peptides in a box with a concentration that mimics the condensate phase, this simulation is representative the experimental PEG-induced condensate systems, hereby referred to as the "excluded volume" or "Excl. Vol" system; 3. The $(GR)_{20}$-RNA system consisting of ten $(GR)_{20}$ peptides with 19 poly-A molecules. All the systems include additional ions to charge balance and to mimic the phosphate buffer concentration used in experiments: 3.8 mM of monobasic and 6.1 mM dibasic phosphate ions. Additionally, K^+ and Cl^- ions were added as much as to neutralize the system. However, it is important to note that folding and secondary structure formation is difficult to reproduce in MD given the long time scales of these processes. Here the simulations were carried out assuming disordered structures, and thus any changes in the environment due to secondary structure are not captured, instead the changes in dynamics observed in simulations is attributed to changes in water dynamics in the condensate compared to the dilute phase. The simulation results primarily illustrate how interactions between poly-A and the peptide influence water dynamics in the condensate. In contrast, the condensate phase with PEG in the experimental section, designed to show only the excluded volume effect, demonstrates the crowded environment in the condensate system isolating effects of the condensate on the local dynamics. In many cases, PEG acts as an inert crowder and is generally excluded from condensates; however, in cases like the NPM1-RNA condensate, PEG has been shown to partition into the condensate.[73,74] Currently, it is unclear as to the sequence-dependent manner that PEG may partition into some condensates but be excluded from others. As PEG is amphiphilic, it may be possible that a balance of charge and hydrophobic sequences is required for PEG partitioning into the condensate.[75] Moreover, highly charged species, like that of coacervates formed from poly-U and spermine, tend to exclude PEG. Given the high charge of poly$(GR)_{20}$, we expect PEG to be generally excluded from the condensate phase, acting primarily as a crowder.[53,74]

The H-bond autocorrelations for the backbone carbonyl groups of the amide I vibrational modes in all three systems indicate a general slowdown in both condensate phases (Figure 5B), consistent with experimental data. The amide C═O H-bond lifetime is 2.6 ps in the dilute phase, while in the Excl.Vol condensate phase, it increases to 3.5 ps, representing an approximate 33% slowdown. Similarly, the H-bond lifetime of the amide mode in the RNA condensate phase is around 5.09 ps, indicating a 93% increase. The charge interactions between poly-A and the arginine side chain primarily influence the H-bond networks within the solvation shells of the peptide. For the C═O groups, the observed slowdown in H-bond lifetimes can primarily be attributed to the disrupted H-bond networks as a result of the localization of poly-A around within the solvation layer of the peptide; moreover, the strong electrostatic interaction of the arginine side chain and phosphate backbone may play also a role in the slowdown. The slowdown in the Excl.Vol system is attributed to the crowded environment of the condensate which disrupts H-bond configurations.[76] Examining the H-bond network in greater detail, the histogram results indicate that the number of H-bonds remains consistent across each system (Figure S11). This consistency suggests that the slowdown in both condensate systems is not due to desolvation. The number of water molecules in the hydration shell remain stable and do not disrupt the balance of H-bond donors and acceptors.

As discussed above, the simulations not fully account for the impact of the protein's secondary structure on the H-bond dynamics of the system, nor do they accurately capture the interactions between PEG and the protein under experimental conditions. Consequently, the degree and order of the system slowdown differs from the experimental data observed in $(GR)_{20}$. However, the MD results effectively capture the general slowdown by tracing the electrostatic interactions and

https://doi.org/10.1021/jacs.4c11226
J. Am. Chem. Soc. 2024, 146, 33616−33625

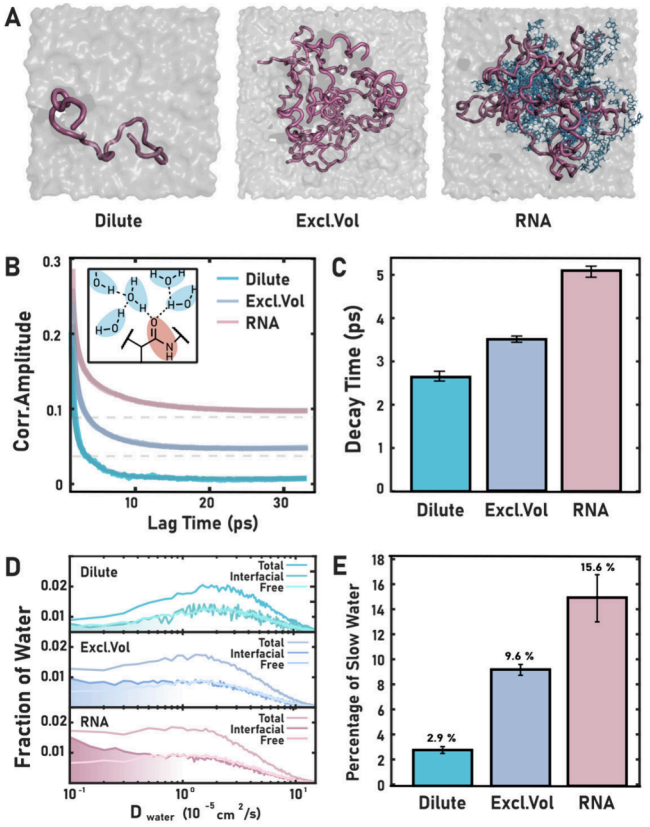

Figure 5. (A) Snapshots of equilibrated MD boxes for each system. (B) Hydrogen bond autocorrelations for the amide backbone, extracted from the MD trajectory and fitted to an exponential curve. (C) H-bond decay times of all three systems are shown, with error bars produced by the second derivative value of each hydrogen bond lifetime computed from each trajectory. (D) A histogram of the water diffusion constants, computed from a mean-square displacement analysis of each simulated system. (E) The population of interfacial water with diffusion coefficients (D) under 0.5 cm^2/s. Error bars represent the second derivative value of the extracted interfacial mean-square displacement values from each trajectory.

excluded volume effects, elucidating their impact on the dynamics of the solvation shell in the condensate phase.

To further characterize the slowdown in water dynamics within the condensate phase observed in the simulations, we computed histograms of the diffusion coefficients extracted from short MD trajectories. Figure 5D shows the diffusion constants of interfacial water (<5 Å) and free water (>5 Å). The 5 Å cutoff for interfacial water is representative of the first two solvation layers surrounding the peptide. The cutoff is arbitrary but guided by a combination of previous literature of amide to water radial distribution functions as well as our own shown in Figure S12. The total distribution in the dilute phase differs from that in the condensate phases, exhibiting increased populations with faster diffusion. In contrast, both Excl.Vol and RNA condensate phases show increased populations with slower diffusion rates for interfacial water, implying that water is more tightly bound or "trapped" within the condensate phase compared to the dilute phase, causing a slowdown in water dynamics. Figure 5E displays the percentage of interfacial water with a diffusion constant (D) below 0.5×10^{-5} cm^2/s. This result indicates the presence of confined water molecules in the condensate systems, particularly the RNA condensate system, which exhibits confined water due to strong electrostatic and H-bonding interactions between the arginine side side chains and the backbone phosphates in RNA. These interactions result in different dynamics in the two condensate systems and likely account for the differences in H-bond lifetimes observed.

CONCLUSION

In summary, we have shown that the dipeptide repeat $(GR)_{20}$, known to cause cyto-toxicity within cells, has distinct secondary structures depending on how the condensate is formed. $(GR)_{20}$ forms a primarily β-sheet structure in a condensate formed by excluded volume effects (PEG) while it forms looplike structures when interacting with RNA. As the mechanisms of cytotoxicity of these dipeptide repeats is believed to be competitive binding for RNA within the cell in combination with mislocalization of similar proteins outside of the nucleolus into protein-rich regions within the cytoplasm, this result offers insight into the molecular structure of phase-separating proteins containing similar sequences such as the mutation caused by C_4G_2 expansion and the RGG-rich domain of FUS protein.[25,28,30,31,77,78] In the context of DPR-related phase separating systems, these results provide a spectroscopic view of the structural differences of condensates formed through protein−protein interactions, and those condensates formed with a RNA or other macromolecular biomolecules. While both regimes see a decrease in the random coil content, the excluded-volume condensate formed through likely form transient β-sheets. Of note, previous studies of similar DPR peptides had shown a length dependence to their cytotoxicity with around 30 repeats found to be toxic to cells; moreover, it is known that longer phase separating peptides form denser condensates.[79,80] These results, in concert with previous cytotoxic studies, could indicate that formation of β-sheet-like character in glycine rich sequences could serve as a nucleation event for condensate aging leading to the aggregation seen in similar biological systems.[77,81,82] Furthermore, we found evidence that in the condensate formed through excluded volume interactions, wherein $(GR)_{20}$ is experiencing an increase in peptide−peptide interactions, the increase in β-sheet character could hint that when similar sequences mislocalize outside of the condensate, the peptides quickly age into an aggregate phase due to the protein-rich environment. Furthermore, as RNA has been shown to prevent FUS from aggregating, we believe that our findings hint that the looped structure of $(GR)_{20}$ in the RNA condensed phase could be important in retaining condensate fluidity and preventing further aggregation due to lack of a nucleation site.[83]

The dynamics in the condensate also differ from that of the dilute phase. In both cases, we have shown that 2D IR spectra show a slowdown in the local dynamics around the peptide backbone carbonyls which correlates with the water-C═O hydrogen bond lifetimes computed from MD simulations. We believe this difference in the dynamics surrounding the amide backbone is largely due to the crowded nature of water confined to nanoscale regions formed through the percolated network of interactions between condensate constituents. Though we are unable to experimentally access longer time scales associated with water diffusion, from the MD simulations, water dynamics are perturbed the most in the condensate formed through attractive interactions between two different biomolecules such as $(GR)_{20}$ and poly-A. This could be due to a combination of the different structures found

https://doi.org/10.1021/jacs.4c11226
J. Am. Chem. Soc. 2024, 146, 33616−33625

within these condensates along with stronger interactions than that of the condensate formed through excluded volume crowding. The combination of strong interactions forming a tight percolated network, and different structures may cause an increase in the population of "bound" water wherein confined water is less dynamic. This higher population of confined water may be the cause of mesoscopic properties of some condensates such as a high viscosity, deformed shapes and slow diffusion.

We have shown that the DPR $(GR)_{20}$ shows interaction-dependent secondary structure formation and dynamics. These differences may hint at the fact that the stability of condensates can be dependent on how the condensate is formed (i.e., through direct interaction vs excluded volume) and potential microscopic differences in biological condensates that contain combinations of biomolecules.[29] Within the context of the $(GR)_{20}$, the fact that there is both experimental and computational evidence for transient β-sheet character in similar poly-GR peptides might suggest that aggregation of this DPR is dependent upon self-interactions and is perturbed by other biomolecules like nucleic acids likely resulting from interactions between the protein side chains and RNA backbone.[34,84] This hypothesis is also supported by similar systems which show reentrant phase behavior with varying concentrations of RNA and preventing aggregation, suggesting that this looped structure is important for the condensate to remain dynamic.[85]

MATERIALS AND METHODS

Sample Preparation. $(GR)_{20}$ was purchased from Genscript (Piscataway, NJ, USA), and was acid lyophilized three times in D_2O with 1% DCl to remove residual TFA from synthesis. Poly-A was purchased from Sigma-Aldrich (MW ranging from 700 to 3500 kDa) with an average of 6 residues per chain. Poly-A, KH_2PO_4 and K_2HPO_4 were lyophilized three times in pure D_2O for the exchange of any protic hydrogens. A 10X Phosphate stock buffer, PBS, was prepared by combining 385 μL of 1 M KH_2PO_4 with 615 μL of 1 M K_2HPO_4 both previously dissolved in D_2O similar to previous studies on similar systems.[32] This stock was brought to a final pH of 7.4 and was not corrected for the deuterium effect.[86] Measurements were done on peptides at a concentration of 500 μM, or approximately 2 mg/mL in 1X PBS. To form the condensates of $(GR)_{20}$ and PEG, the peptide was measured at 500 μM in 30% v/v PEG and 1X PBS. To form the condensates of $(GR)_{20}$ and poly-A, the peptide was measured at 500 μM in 1X PBS and 2 mg/mL poly-A.

2D Infrared Spectroscopy. 2DIR spectra were measured using a custom-built spectrometer described in detail previously.[59] In short, the spectra were obtained by generating a sequence of three 100 fs pulses centered around 6 μm. The two excitation pulses are used to resolve the excitation frequency axis, and the detection pulse is directly measured using a dispersive spectrometer equipped with a 128 × 128-element MCT array. The excitation pulses are generated using a pulse shaper (Phase Tech Inc.), and the excitation frequencies are generated by Fourier transforming the time delay between the two pulses. The excitation and detection pulses were in perpendicular polarization to suppress scatter. Spectra were measured at waiting times ranging from 150 to 2000 fs with a negative time delay spectra taken for scatter subtraction from the condensate spectra due to heavy scattering from the sample.

Molecular Dynamics Simulations. Initial $(GR)_{20}$ peptide conformations were generated using the IDPConfGen software, which produces random conformations based on a distribution of backbone angles extracted from sequence analogues within a PDB database.[87] A total of ten disordered $(GR)_{20}$ peptide configurations were generated and protonated, with each peptide carrying a + 20 charge from the arginine side-chains.

To generate random poly-A RNA conformations, a six-residue poly-A RNA structure was generated using RNA Composer, which designs 3D RNA models based on machine translation principles.[88,89] A single poly-A structure, with each backbone phosphate carrying a −1 charge, was randomly packed with 2809 water molecules, and 5 potassium ions were added to neutralize the system using PackMol software.[90] The CHARMM 36 force field was applied to all components, with water molecules modeled using CHARMM-TIP3P.[91] The initial system conformation was energy-minimized and equilibrated in an NVT ensemble for 1 ns using the Nose-Hoover thermostat at 300 K with a 1 fs integration time-step. Subsequent equilibration was performed in an NPT ensemble for 1 ns using the Nose-Hoover thermostat and the Parrinello−Rahman barostat, with a 2 ps integration time-step.[92] Bonds with hydrogen atoms were restricted by using the LINCS algorithm. The 10 ns production trajectory was generated with the same settings as the NPT equilibration. From the final trajectory, 19 poly-A residues were generated for the condensate system simulation.

Three systems were constructed for the $(GR)_{20}$ MD simulations for comparison to the experimental conditions: the dilute phase, the condensate phase with RNA, and the condensate phase with protein only (solely $(GR)_{20}$). In the dilute phase system, a single $(GR)_{20}$ peptide was packed using PackMol software, along with 20 chloride ions to neutralize the peptide charge and 4000 water molecules to fill the box. To replicate experimental buffer conditions, phosphate ions were added, including two monobasic phosphate ions, one dibasic ion, and five potassium ions.

For the second system, which included $(GR)_{20}$ and poly-A residues in a 1:1.9 ratio, ten $(GR)_{20}$ peptides (+20 charge each) were generated using the IDPConfGen software. Nineteen Poly-A residues (−5 charge each) were extracted from the poly-A MD production trajectory. Phosphate ions were added to mimic the buffer solution, including 12 monobasic ($H_2PO_4^-$) and 19 dibasic phosphate (HPO_4^{2-}) ions. To balance the system's charge, 200 chloride ions and 195 potassium ions were added. This system underwent the same conditions as the poly-A MD simulation process.

The third system simulates an excluded volume effect by omitting poly-A molecules to maintain conditions similar to the $(GR)_{20}$ with the poly-A condensate phase, instead of simulating a system with PEG. The trajectory from the $(GR)_{20}$ with poly-A condensate phase after the NPT equilibration step was used as a starting point. All 19 poly-A molecules and 95 potassium ions neutralizing the molecules were removed from the. pdb file. As the starting system was already energy minimized and NVT equilibrated, a 1 ns NPT equilibration step was performed with a 2 fs integration time step, followed by a 100 ns MD production run under the same conditions as the previous simulations. For further analysis, snapshots were saved every 10 ns from the final trajectory of all three systems. All simulations were performed using the GROMACS 2021.3 package.[93−95]

To conduct further H-bond analysis of the system, snapshots saved previously served as starting points for 2 fs time step short production run. H-bond analysis was then performed using the MDAnalysis package, with a donor−acceptor cutoff distance of 0.3 nm and a donor−acceptor-hydrogen cutoff angle of 150 degrees.[96,97] The H-bond lifetimes were extracted from the MD production results by computing the autocorrelation of the H-bond trajectory for each short run. This analysis includes the C═O groups from the peptide backbone. The autocorrelation data were then fitted to a multi-exponential model using MATLAB R2022.b.

Water diffusion constants for each short run were obtained by linearly fitting the mean-squared displacement of the TIP3P water over 10 ps windows, utilizing the "msd" tool in GROMACS 2021.3.

ASSOCIATED CONTENT

Supporting Information

The Supporting Information is available free of charge at https://pubs.acs.org/doi/10.1021/jacs.4c11226.

Microscope images of each $(GR)_{20}$ system tested, size distributions of the condensates, 2D IR spectra of each

https://doi.org/10.1021/jacs.4c11226
J. Am. Chem. Soc. 2024, 146, 33616−33625

system including a poly-A spectrum, overlapped PSAs along with a detailed description of PSA, detailed description of the secondary structure fitting analysis and fitting results, AlphaFold3 predicted structures and predicted spectra, detailed description of CLS and the CLS fitting results, MD simulation boxes, MD H-bond autocorrelation results, amide H-bond histograms, and amide oxygen to water oxygen radial distribution functions (PDF)

AUTHOR INFORMATION

Corresponding Author

Carlos R. Baiz − *Department of Chemistry, University of Texas at Austin, Austin, Texas 78712, United States;* orcid.org/0000-0003-0699-8468; Email: cbaiz@cm.utexas.edu

Authors

Keegan A. Lorenz-Ochoa − *Department of Chemistry, University of Texas at Austin, Austin, Texas 78712, United States*

Moonyeon Cho − *Department of Chemistry, University of Texas at Austin, Austin, Texas 78712, United States*

Sapun H. Parekh − *Department of Biomedical Engineering, University of Texas at Austin, Austin, Texas 78712, United States;* orcid.org/0000-0001-8522-1854

Complete contact information is available at: https://pubs.acs.org/10.1021/jacs.4c11226

Notes

The authors declare no competing financial interest.

ACKNOWLEDGMENTS

C.B. acknowledges support from the National Institutes of Health (R35GM133359), the Welch Foundation (F-1891), and Camille and Henry Dreyfus Foundation. S.P. acknowledges support from the National Science Foundation (2146549) and the Welch Foundation (F-2008-20220331). Simulations were carried out using the Texas Advanced Computing Center (TACC) Lonestar6 cluster. Imaging was performed at the Center for Biomedical Research Support Microscopy and Imaging Facility at UT Austin (RRID# SCR_021756).

REFERENCES

(1) Banani, S. F.; Lee, H. O.; Hyman, A. A.; Rosen, M. K. Biomolecular Condensates: Organizers of Cellular Biochemistry. *Nat. Rev. Mol. Cell Biol.* **2017**, *18* (5), 285−298.

(2) Hyman, A. A.; Weber, C. A.; Jülicher, F. Liquid-Liquid Phase Separation in Biology. *Annu. Rev. Cell Dev. Biol.* **2014**, *30* (1), 39−58.

(3) Mitrea, D. M.; Chandra, B.; Ferrolino, M. C.; Gibbs, E. B.; Tolbert, M.; White, M. R.; Kriwacki, R. W. Methods for Physical Characterization of Phase-Separated Bodies and Membrane-Less Organelles. *J. Mol. Biol.* **2018**, *430* (23), 4773−4805.

(4) Alberti, S.; Gladfelter, A.; Mittag, T. Considerations and Challenges in Studying Liquid-Liquid Phase Separation and Biomolecular Condensates. *Cell* **2019**, *176* (3), 419−434.

(5) Dignon, G. L.; Best, R. B.; Mittal, J. Biomolecular Phase Separation: From Molecular Driving Forces to Macroscopic Properties. *Annu. Rev. Phys. Chem.* **2020**, *71* (1), 53−75.

(6) O'Flynn, B. G.; Mittag, T. The Role of Liquid−Liquid Phase Separation in Regulating Enzyme Activity. *Curr. Opin. Cell Biol.* **2021**, *69*, 70−79.

(7) Wei, M.-T.; Elbaum-Garfinkle, S.; Holehouse, A. S.; Chen, C. C.-H.; Feric, M.; Arnold, C. B.; Priestley, R. D.; Pappu, R. V.; Brangwynne, C. P. Phase Behaviour of Disordered Proteins Underlying Low Density and High Permeability of Liquid Organelles. *Nat. Chem.* **2017**, *9* (11), 1118−1125.

(8) Tesei, G.; Schulze, T. K.; Crehuet, R.; Lindorff-Larsen, K. Accurate Model of Liquid−Liquid Phase Behavior of Intrinsically Disordered Proteins from Optimization of Single-Chain Properties. *Proc. Natl. Acad. Sci. U. S. A.* **2021**, *118* (44), No. e2111696118.

(9) Shen, Z.; Jia, B.; Xu, Y.; Wessén, J.; Pal, T.; Chan, H. S.; Du, S.; Zhang, M. Biological Condensates Form Percolated Networks with Molecular Motion Properties Distinctly Different from Dilute Solutions. *eLife* **2023**, *12*, No. e81907.

(10) Espinosa, J. R.; Joseph, J. A.; Sanchez-Burgos, I.; Garaizar, A.; Frenkel, D.; Collepardo-Guevara, R. Liquid Network Connectivity Regulates the Stability and Composition of Biomolecular Condensates with Many Components. *Proc. Natl. Acad. Sci. U. S. A.* **2020**, *117* (24), 13238−13247.

(11) Schmit, J. D.; Bouchard, J. J.; Martin, E. W.; Mittag, T. Protein Network Structure Enables Switching between Liquid and Gel States. *J. Am. Chem. Soc.* **2020**, *142* (2), 874−883.

(12) Pappu, R. V.; Cohen, S. R.; Dar, F.; Farag, M.; Kar, M. Phase Transitions of Associative Biomacromolecules. *Chem. Rev.* **2023**, *123*, 8945.

(13) Boeynaems, S.; Chong, S.; Gsponer, J.; Holt, L.; Milovanovic, D.; Mitrea, D. M.; Mueller-Cajar, O.; Portz, B.; Reilly, J. F.; Reinkemeier, C. D.; Sabari, B. R.; Sanulli, S.; Shorter, J.; Sontag, E.; Strader, L.; Stachowiak, J.; Weber, S. C.; White, M.; Zhang, H.; Zweckstetter, M.; Elbaum-Garfinkle, S.; Kriwacki, R. Phase Separation in Biology and Disease; Current Perspectives and Open Questions. *J. Mol. Biol.* **2023**, *435* (5), No. 167971.

(14) Vernon, R. M.; Chong, P. A.; Tsang, B.; Kim, T. H.; Bah, A.; Farber, P.; Lin, H.; Forman-Kay, J. D. Pi-Pi Contacts Are an Overlooked Protein Feature Relevant to Phase Separation. *eLife* **2018**, *7*, No. e31486.

(15) Gomes, E.; Shorter, J. The Molecular Language of Membraneless Organelles. *J. Biol. Chem.* **2019**, *294* (18), 7115−7127.

(16) Lorenz-Ochoa, K. A.; Baiz, C. R. Ultrafast Spectroscopy Reveals Slow Water Dynamics in Biocondensates. *J. Am. Chem. Soc.* **2023**, *145*, 27800.

(17) Ahlers, J.; Adams, E. M.; Bader, V.; Pezzotti, S.; Winklhofer, K. F.; Tatzelt, J.; Havenith, M. The Key Role of Solvent in Condensation: Mapping Water in Liquid-Liquid Phase-Separated FUS. *Biophys. J.* **2021**, *120* (7), 1266−1275.

(18) Krevert, C. S.; Chavez, D.; Chatterjee, S.; Stelzl, L. S.; Pütz, S.; Roeters, S. J.; Rudzinski, J. F.; Fawzi, N. L.; Girard, M.; Parekh, S. H.; Hunger, J. Liquid−Liquid Phase Separation of the Intrinsically Disordered Domain of the Fused in Sarcoma Protein Results in Substantial Slowing of Hydration Dynamics. *J. Phys. Chem. Lett.* **2023**, *14* (49), 11224−11234.

(19) Farag, M.; Cohen, S. R.; Borcherds, W. M.; Bremer, A.; Mittag, T.; Pappu, R. V. Condensates Formed by Prion-like Low-Complexity Domains Have Small-World Network Structures and Interfaces Defined by Expanded Conformations. *Nat. Commun.* **2022**, *13* (1), 7722.

(20) Molliex, A.; Temirov, J.; Lee, J.; Coughlin, M.; Kanagaraj, A. P.; Kim, H. J.; Mittag, T.; Taylor, J. P. Phase Separation by Low Complexity Domains Promotes Stress Granule Assembly and Drives Pathological Fibrillization. *Cell* **2015**, *163* (1), 123−133.

(21) Chong, P. A.; Vernon, R. M.; Forman-Kay, J. D. RGG/RG Motif Regions in RNA Binding and Phase Separation. *J. Mol. Biol.* **2018**, *430* (23), 4650−4665.

(22) Boeynaems, S.; De Decker, M.; Tompa, P.; Van Den Bosch, L. Arginine-Rich Peptides Can Actively Mediate Liquid-Liquid Phase Separation. *BIO-Protoc.* **2017**, *7* (17), 1.

(23) Balendra, R.; Ruiz de los Mozos, I.; Odeh, H. M; Glaria, I.; Milioto, C.; Wilson, K. M; Ule, A. M; Hallegger, M.; Masino, L.; Martin, S.; Patani, R.; Shorter, J.; Ule, J.; Isaacs, A. M Transcriptome-

Wide RNA Binding Analysis of C9orf72 Poly(PR) Dipeptides. *Life Sci. Alliance* **2023**, *6* (9), e202201824.
(24) Boeynaems, S.; Bogaert, E.; Kovacs, D.; Konijnenberg, A.; Timmerman, E.; Volkov, A.; Guharoy, M.; De Decker, M.; Jaspers, T.; Ryan, V. H.; Janke, A. M.; Baatsen, P.; Vercruysse, T.; Kolaitis, R.-M.; Daelemans, D.; Taylor, J. P.; Kedersha, N.; Anderson, P.; Impens, F.; Sobott, F.; Schymkowitz, J.; Rousseau, F.; Fawzi, N. L.; Robberecht, W.; Van Damme, P.; Tompa, P.; Van Den Bosch, L. Phase Separation of C9orf72 Dipeptide Repeats Perturbs Stress Granule Dynamics. *Mol. Cell* **2017**, *65* (6), 1044−1055.e5.
(25) Frottin, F.; Pérez-Berlanga, M.; Hartl, F. U.; Hipp, M. S. Multiple Pathways of Toxicity Induced by C9orf72 Dipeptide Repeat Aggregates and G4C2 RNA in a Cellular Model. *eLife* **2021**, *10*, No. e62718.
(26) Raguseo, F.; Wang, Y.; Li, J.; Petrić Howe, M.; Balendra, R.; Huyghebaert, A.; Vadukul, D. M.; Tanase, D. A.; Maher, T. E.; Malouf, L.; Rubio-Sánchez, R.; Aprile, F. A.; Elani, Y.; Patani, R.; Di Michele, L.; Di Antonio, M. The ALS/FTD-Related C9orf72 Hexanucleotide Repeat Expansion Forms RNA Condensates through Multimolecular G-Quadruplexes. *Nat. Commun.* **2023**, *14* (1), 8272.
(27) Smeyers, J.; Banchi, E.-G.; Latouche, M. C9ORF72: What It Is, What It Does, and Why It Matters. *Front. Cell. Neurosci.* **2021**, *15*, 1.
(28) Mizielinska, S.; Grönke, S.; Niccoli, T.; Ridler, C. E.; Clayton, E. L.; Devoy, A.; Moens, T.; Norona, F. E.; Woollacott, I. O. C.; Pietrzyk, J.; Cleverley, K.; Nicoll, A. J.; Pickering-Brown, S.; Dols, J.; Cabecinha, M.; Hendrich, O.; Fratta, P.; Fisher, E. M. C.; Partridge, L.; Isaacs, A. M. C9orf72 Repeat Expansions Cause Neurodegeneration in Drosophila through Arginine-Rich Proteins. *Science* **2014**, *345* (6201), 1192−1194.
(29) Boeynaems, S.; Holehouse, A. S.; Weinhardt, V.; Kovacs, D.; Van Lindt, J.; Larabell, C.; Van Den Bosch, L.; Das, R.; Tompa, P. S.; Pappu, R. V.; Gitler, A. D. Spontaneous Driving Forces Give Rise to protein−RNA Condensates with Coexisting Phases and Complex Material Properties. *Proc. Natl. Acad. Sci. U. S. A.* **2019**, *116* (16), 7889−7898.
(30) Jafarinia, H.; Van der Giessen, E.; Onck, P. R. C9orf72 polyPR Directly Binds to Various Nuclear Transport Components. *eLife* **2024**, *12*, RP89694.
(31) Chen, C.; Yamanaka, Y.; Ueda, K.; Li, P.; Miyagi, T.; Harada, Y.; Tezuka, S.; Narumi, S.; Sugimoto, M.; Kuroda, M.; Hayamizu, Y.; Kanekura, K. Phase Separation and Toxicity of C9orf72 Poly(PR) Depends on Alternate Distribution of Arginine. *J. Cell Biol.* **2021**, *220* (11), No. e202103160.
(32) Edun, D. N.; Flanagan, M. R.; Serrano, A. L. Does Liquid−Liquid Phase Separation Drive Peptide Folding? *Chem. Sci.* **2021**, *12* (7), 2474−2479.
(33) Vanneste, J.; Vercruysse, T.; Boeynaems, S.; Sicart, A.; Van Damme, P.; Daelemans, D.; Van Den Bosch, L. C9orf72-Generated Poly-GR and Poly-PR Do Not Directly Interfere with Nucleocytoplasmic Transport. *Sci. Rep.* **2019**, *9*, No. 15728.
(34) Zheng, S.; Sahimi, A.; Shing, K. S.; Sahimi, M. Molecular Dynamics Study of Structure, Folding, and Aggregation of Poly-PR and Poly-GR Proteins. *Biophys. J.* **2021**, *120* (1), 64−72.
(35) Das, S.; Lin, Y.-H.; Vernon, R. M.; Forman-Kay, J. D.; Chan, H. S. Comparative Roles of Charge, π, and Hydrophobic Interactions in Sequence-Dependent Phase Separation of Intrinsically Disordered Proteins. *Proc. Natl. Acad. Sci. U. S. A.* **2020**, *117* (46), 28795−28805.
(36) Kausik, R.; Srivastava, A.; Korevaar, P. A.; Stucky, G.; Waite, J. H.; Han, S. Local Water Dynamics in Coacervated Polyelectrolytes Monitored through Dynamic Nuclear Polarization-Enhanced 1H NMR. *Macromolecules* **2009**, *42* (19), 7404−7412.
(37) Hazra, M. K.; Levy, Y. Biophysics of Phase Separation of Disordered Proteins Is Governed by Balance between Short- And Long-Range Interactions. *J. Phys. Chem. B* **2021**, *125* (9), 2202−2211.
(38) Tan, C.; Niitsu, A.; Sugita, Y. Highly Charged Proteins and Their Repulsive Interactions Antagonize Biomolecular Condensation. *JACS Au* **2023**, *3* (3), 834−848.
(39) Ghosh, A.; Ostrander, J. S.; Zanni, M. T. Watching Proteins Wiggle: Mapping Structures with Two-Dimensional Infrared Spectroscopy. *Chem. Rev.* **2017**, *117* (16), 10726−10759.
(40) Bagchi, S.; Falvo, C.; Mukamel, S.; Hochstrasser, R. M. 2D-IR Experiments and Simulations of the Coupling between Amide-I and Ionizable Side Chains in Proteins: Application to the Villin Headpiece. *J. Phys. Chem. B* **2009**, *113* (32), 11260−11273.
(41) Demirdöven, N.; Cheatum, C. M.; Chung, H. S.; Khalil, M.; Knoester, J.; Tokmakoff, A. Two-Dimensional Infrared Spectroscopy of Antiparallel β-Sheet Secondary Structure. *J. Am. Chem. Soc.* **2004**, *126* (25), 7981−7990.
(42) Thielges, M. C.; Fayer, M. D. Protein Dynamics Studied with Ultrafast Two-Dimensional Infrared Vibrational Echo Spectroscopy. *Acc. Chem. Res.* **2012**, *45* (11), 1866−1874.
(43) Hamm, P.; Lim, M.; Hochstrasser, R. M. Structure of the Amide I Band of Peptides Measured by Femtosecond Nonlinear-Infrared Spectroscopy. *J. Phys. Chem. B* **1998**, *102* (31), 6123−6138.
(44) Choi, J.-H.; Raleigh, D.; Cho, M. Azido Homoalanine Is a Useful Infrared Probe for Monitoring Local Electrostatistics and Side-Chain Solvation in Proteins. *J. Phys. Chem. Lett.* **2011**, *2* (17), 2158−2162.
(45) Chen, X.; Roeters, S.; Cavanna, F.; Alvarado, J.; Baiz, C. Crowding Alters F-Actin Secondary Structure and Hydration. *ChemRxiv* **2023**; DOI: 10.26434/chemrxiv-2023-b88nb.
(46) Laage, D.; Elsaesser, T.; Hynes, J. T. Water Dynamics in the Hydration Shells of Biomolecules. *Chem. Rev.* **2017**, *117* (16), 10694−10725.
(47) Hamm, P.; Woutersen, S. Coupling of the Amide I Modes of the Glycine Dipeptide. *Bull. Chem. Soc. Jpn.* **2002**, *75* (5), 985−988.
(48) Baiz, C. R.; Peng, C. S.; Reppert, M. E.; Jones, K. C.; Tokmakoff, A. Coherent Two-Dimensional Infrared Spectroscopy: Quantitative Analysis of Protein Secondary Structure in Solution. *Analyst* **2012**, *137* (8), 1793−1799.
(49) de Boeij, W. P.; Pshenichnikov, M. S.; Wiersma, D. A. Ultrafast Solvation Dynamics Explored by Femtosecond Photon Echo Spectroscopies. *Annu. Rev. Phys. Chem.* **1998**, *49* (1), 99−123.
(50) Peng, C. S.; Jones, K. C.; Tokmakoff, A. Anharmonic Vibrational Modes of Nucleic Acid Bases Revealed by 2D IR Spectroscopy. *J. Am. Chem. Soc.* **2011**, *133* (39), 15650−15660.
(51) You, X.; Shirley, J. C.; Lee, E.; Baiz, C. R. Short- and Long-Range Crowding Effects on Water's Hydrogen Bond Networks. *Cell Rep. Phys. Sci.* **2021**, *2* (5), No. 100419.
(52) Shirley, J. C.; Baiz, C. R. Local Crowd, Local Probe: Strengths and Drawbacks of Azidohomoalanine as a Site-Specific Crowding Probe. *J. Phys. Chem. B* **2024**, *128* (22), 5310−5319.
(53) Poudyal, M.; Patel, K.; Gadhe, L.; Sawner, A. S.; Kadu, P.; Datta, D.; Mukherjee, S.; Ray, S.; Navalkar, A.; Maiti, S.; Chatterjee, D.; Devi, J.; Bera, R.; Gahlot, N.; Joseph, J.; Padinhateeri, R.; Maji, S. K. Intermolecular Interactions Underlie Protein/Peptide Phase Separation Irrespective of Sequence and Structure at Crowded Milieu. *Nat. Commun.* **2023**, *14* (1), 6199.
(54) Cinar, H.; Winter, R. The Effects of Cosolutes and Crowding on the Kinetics of Protein Condensate Formation Based on Liquid−Liquid Phase Separation: A Pressure-Jump Relaxation Study. *Sci. Rep.* **2020**, *10* (1), No. 17245.
(55) Baiz, C. R.; Reppert, M.; Tokmakoff, A. Amide I Two-Dimensional Infrared Spectroscopy: Methods for Visualizing the Vibrational Structure of Large Proteins. *J. Phys. Chem. A* **2013**, *117* (29), 5955−5961.
(56) Ghosh, A.; Tucker, M. J.; Hochstrasser, R. M. Identification of Arginine Residues in Peptides by 2D-IR Echo Spectroscopy. *J. Phys. Chem. A* **2011**, *115* (34), 9731−9738.
(57) Vorobyev, D. Yu.; Kuo, C.-H.; Chen, J.-X.; Kuroda, D. G.; Scott, J. N.; Vanderkooi, J. M.; Hochstrasser, R. M. Ultrafast Vibrational Spectroscopy of a Degenerate Mode of Guanidinium Chloride. *J. Phys. Chem. B* **2009**, *113* (46), 15382−15391.
(58) Valentine, M. L.; Al-Mualem, Z. A.; Baiz, C. R. Pump Slice Amplitudes: A Simple and Robust Method for Connecting Two-

Dimensional Infrared and Fourier Transform Infrared Spectra. *J. Phys. Chem. A* **2021**, *125* (29), 6498−6504.
(59) Edington, S. C.; Gonzalez, A.; Middendorf, T. R.; Halling, D. B.; Aldrich, R. W.; Baiz, C. R. Coordination to Lanthanide Ions Distorts Binding Site Conformation in Calmodulin. *Proc. Natl. Acad. Sci. U. S. A.* **2018**, *115* (14), E3126−E3134.
(60) Alasadi, E. A.; Choi, W.; Chen, X.; Cotruvo, J. A. J.; Baiz, C. R. Lanmodulin's EF 2−3 Domain: Insights from Infrared Spectroscopy and Simulations. *ACS Chem. Biol.* **2024**, *19* (5), 1056−1065.
(61) Weeks, W. B.; Buchanan, L. E. Label-Free Detection of β-Sheet Polymorphism. *J. Phys. Chem. Lett.* **2022**, *13* (40), 9534−9538.
(62) Oh, K.-I.; Rajesh, K.; Stanton, J. F.; Baiz, C. R. Quantifying Hydrogen-Bond Populations in Dimethyl Sulfoxide/Water Mixtures. *Angew. Chem.* **2017**, *129* (38), 11533−11537.
(63) You, X.; Lee, E.; Xu, C.; Baiz, C. R. Molecular Mechanism of Cell Membrane Protection by Sugars: A Study of Interfacial H-Bond Networks. *J. Phys. Chem. Lett.* **2021**, *12* (39), 9602−9607.
(64) Lee, C.; Cho, M. Local Amide I Mode Frequencies and Coupling Constants in Multiple-Stranded Antiparallel β-Sheet Polypeptides. *J. Phys. Chem. B* **2004**, *108* (52), 20397−20407.
(65) Ganim, Z.; Chung, H. S.; Smith, A. W.; DeFlores, L. P.; Jones, K. C.; Tokmakoff, A. Amide I Two-Dimensional Infrared Spectroscopy of Proteins. *Acc. Chem. Res.* **2008**, *41* (3), 432−441.
(66) Abramson, J.; Adler, J.; Dunger, J.; Evans, R.; Green, T.; Pritzel, A.; Ronneberger, O.; Willmore, L.; Ballard, A. J.; Bambrick, J.; Bodenstein, S. W.; Evans, D. A.; Hung, C.-C.; O'Neill, M.; Reiman, D.; Tunyasuvunakool, K.; Wu, Z.; Žemgulytė, A.; Arvaniti, E.; Beattie, C.; Bertolli, O.; Bridgland, A.; Cherepanov, A.; Congreve, M.; Cowen-Rivers, A. I.; Cowie, A.; Figurnov, M.; Fuchs, F. B.; Gladman, H.; Jain, R.; Khan, Y. A.; Low, C. M. R.; Perlin, K.; Potapenko, A.; Savy, P.; Singh, S.; Stecula, A.; Thillaisundaram, A.; Tong, C.; Yakneen, S.; Zhong, E. D.; Zielinski, M.; Žídek, A.; Bapst, V.; Kohli, P.; Jaderberg, M.; Hassabis, D.; Jumper, J. M. Accurate Structure Prediction of Biomolecular Interactions with AlphaFold 3. *Nature* **2024**, *630* (8016), 493−500.
(67) Roberts, S. T.; Loparo, J. J.; Tokmakoff, A. Characterization of Spectral Diffusion from Two-Dimensional Line Shapes. *J. Chem. Phys.* **2006**, *125* (8), No. 084502.
(68) Kramer, P. L.; Nishida, J.; Fayer, M. D. Separation of Experimental 2D IR Frequency-Frequency Correlation Functions into Structural and Reorientation-Induced Contributions. *J. Chem. Phys.* **2015**, *143* (12), No. 124505.
(69) Kwak, K.; Park, S.; Finkelstein, I. J.; Fayer, M. D. Frequency-Frequency Correlation Functions and Apodization in Two-Dimensional Infrared Vibrational Echo Spectroscopy: A New Approach. *J. Chem. Phys.* **2007**, *127* (12), No. 124503.
(70) Salamatova, E.; Cunha, A. V.; Bloem, R.; Roeters, S. J.; Woutersen, S.; Jansen, T. L. C.; Pshenichnikov, M. S. Hydrophobic Collapse in N-Methylacetamide−Water Mixtures. *J. Phys. Chem. A* **2018**, *122* (9), 2468−2478.
(71) Cunha, A. V.; Salamatova, E.; Bloem, R.; Roeters, S. J.; Woutersen, S.; Pshenichnikov, M. S.; Jansen, T. L. C. Interplay between Hydrogen Bonding and Vibrational Coupling in Liquid N-Methylacetamide. *J. Phys. Chem. Lett.* **2017**, *8* (11), 2438−2444.
(72) Woutersen, S.; Pfister, R.; Hamm, P.; Mu, Y.; Kosov, D. S.; Stock, G. Peptide Conformational Heterogeneity Revealed from Nonlinear Vibrational Spectroscopy and Molecular-Dynamics Simulations. *J. Chem. Phys.* **2002**, *117* (14), 6833−6840.
(73) André, A. A. M.; Yewdall, N. A.; Spruijt, E. Crowding-Induced Phase Separation and Gelling by Co-Condensation of PEG in NPM1-rRNA Condensates. *Biophys. J.* **2023**, *122* (2), 397−407.
(74) Marianelli, A. M.; Miller, B. M.; Keating, C. D. Impact of Macromolecular Crowding on RNA/Spermine Complex Coacervation and Oligonucleotide Compartmentalization. *Soft Matter* **2018**, *14* (3), 368−378.
(75) Parray, Z. A.; Hassan, M. I.; Ahmad, F.; Islam, A. Amphiphilic Nature of Polyethylene Glycols and Their Role in Medical Research. *Polym. Test.* **2020**, *82*, No. 106316.
(76) You, X.; Baiz, C. R. Importance of Hydrogen Bonding in Crowded Environments: A Physical Chemistry Perspective. *J. Phys. Chem. A* **2022**, *126* (35), 5881−5889.
(77) Cook, C. N.; Wu, Y.; Odeh, H. M.; Gendron, T. F.; Jansen-West, K.; del Rosso, G.; Yue, M.; Jiang, P.; Gomes, E.; Tong, J.; Daughrity, L. M.; Avendano, N. M.; Castanedes-Casey, M.; Shao, W.; Oskarsson, B.; Tomassy, G. S.; McCampbell, A.; Rigo, F.; Dickson, D. W.; Shorter, J.; Zhang, Y.-J.; Petrucelli, L. C9orf72 Poly(GR) Aggregation Induces TDP-43 Proteinopathy. *Sci. Transl. Med.* **2020**, *12* (559), No. eabb3774.
(78) White, M. R.; Mitrea, D. M.; Zhang, P.; Stanley, C. B.; Cassidy, D. E.; Nourse, A.; Phillips, A. H.; Tolbert, M.; Taylor, J. P.; Kriwacki, R. W. C9orf72 Poly(PR) Dipeptide Repeats Disturb Biomolecular Phase Separation and Disrupt Nucleolar Function. *Mol. Cell* **2019**, *74* (4), 713−728.e6.
(79) Li, L.; Srivastava, S.; Andreev, M.; Marciel, A. B.; de Pablo, J. J.; Tirrell, M. V. Phase Behavior and Salt Partitioning in Polyelectrolyte Complex Coacervates. *Macromolecules* **2018**, *51* (8), 2988−2995.
(80) Jafarinia, H.; van der Giessen, E.; Onck, P. R. Phase Separation of Toxic Dipeptide Repeat Proteins Related to C9orf72 ALS/FTD. *Biophys. J.* **2020**, *119* (4), 843−851.
(81) Fare, C. M.; Villani, A.; Drake, L. E.; Shorter, J. Higher-Order Organization of Biomolecular Condensates. *Open Biol.* **2021**, DOI: 10.1098/rsob.210137.
(82) Schwartz, J. C.; Wang, X.; Podell, E. R.; Cech, T. R. RNA Seeds Higher-Order Assembly of FUS Protein. *Cell Rep.* **2013**, *5* (4), 918−925.
(83) Maharana, S.; Wang, J.; Papadopoulos, D. K.; Richter, D.; Pozniakovsky, A.; Poser, I.; Bickle, M.; Rizk, S.; Guillén-Boixet, J.; Franzmann, T. M.; Jahnel, M.; Marrone, L.; Chang, Y.-T.; Sterneckert, J.; Tomancak, P.; Hyman, A. A.; Alberti, S. RNA Buffers the Phase Separation Behavior of Prion-like RNA Binding Proteins. *Science* **2018**, *360* (6391), 918−921.
(84) Phan, A. T.; Kuryavyi, V.; Darnell, J. C.; Serganov, A.; Majumdar, A.; Ilin, S.; Raslin, T.; Polonskaia, A.; Chen, C.; Clain, D.; Darnell, R. B.; Patel, D. J. Structure-Function Studies of FMRP RGG Peptide Recognition of an RNA Duplex-Quadruplex Junction. *Nat. Struct. Mol. Biol.* **2011**, *18* (7), 796−804.
(85) Banerjee, P. R.; Milin, A. N.; Moosa, M. M.; Onuchic, P. L.; Deniz, A. A. Reentrant Phase Transition Drives Dynamic Substructure Formation in Ribonucleoprotein Droplets. *Angew. Chem., Int. Ed.* **2017**, *56* (38), 11354−11359.
(86) Krężel, A.; Bal, W. A Formula for Correlating pKa Values Determined in D2O and H2O. *J. Inorg. Biochem.* **2004**, *98* (1), 161−166.
(87) Teixeira, J. M. C.; Liu, Z. H.; Namini, A.; Li, J.; Vernon, R. M.; Krzeminski, M.; Shamandy, A. A.; Zhang, O.; Haghighatlari, M.; Yu, L.; Head-Gordon, T.; Forman-Kay, J. D. IDPConformerGenerator: A Flexible Software Suite for Sampling the Conformational Space of Disordered Protein States. *J. Phys. Chem. A* **2022**, *126* (35), 5985−6003.
(88) Sarzynska, J.; Popenda, M.; Antczak, M.; Szachniuk, M. RNA Tertiary Structure Prediction Using RNAComposer in CASP15. *Proteins Struct. Funct. Bioinforma.* **2023**, *91* (12), 1790−1799.
(89) Popenda, M.; Szachniuk, M.; Antczak, M.; Purzycka, K. J.; Lukasiak, P.; Bartol, N.; Blazewicz, J.; Adamiak, R. W. Automated 3D Structure Composition for Large RNAs. *Nucleic Acids Res.* **2012**, *40* (14), e112−e112.
(90) Martínez, L.; Andrade, R.; Birgin, E. G.; Martínez, J. M. P ACKMOL: A Package for Building Initial Configurations for Molecular Dynamics Simulations. *J. Comput. Chem.* **2009**, *30* (13), 2157−2164.
(91) Jo, S.; Kim, T.; Iyer, V. G.; Im, W. CHARMM-GUI: A Web-based Graphical User Interface for CHARMM. *J. Comput. Chem.* **2008**, *29* (11), 1859−1865.
(92) Cheng, A.; Merz, K. M. Application of the Nosé−Hoover Chain Algorithm to the Study of Protein Dynamics. *J. Phys. Chem.* **1996**, *100* (5), 1927−1937.

(93) Abraham, M.; Alekseenko, A.; Basov, V.; Bergh, C.; Briand, E.; Brown, A.; Doijade, M.; Fiorin, G.; Fleischmann, S.; Gorelov, S.; Gouaillardet, G.; Grey, A.; Irrgang, M. E.; Jalalypour, F.; Jordan, J.; Kutzner, C.; Lemkul, J. A.; Lundborg, M.; Merz, P.; Miletic, V.; Morozov, D.; Nabet, J.; Pall, S.; Pasquadibisceglie, A.; Pellegrino, M.; Santuz, H.; Schulz, R.; Shugaeva, T.; Shvetsov, A.; Villa, A.; Wingbermuehle, S.; Hess, B.; Lindahl, E. *GROMACS 2024.2 Manual*; 2024; DOI: 10.5281/ZENODO.11148638.
(94) Berendsen, H. J. C.; Van Der Spoel, D.; Van Drunen, R. GROMACS: A Message-Passing Parallel Molecular Dynamics Implementation. *Comput. Phys. Commun.* **1995**, *91* (1−3), 43−56.
(95) Van Der Spoel, D.; Lindahl, E.; Hess, B.; Groenhof, G.; Mark, A. E.; Berendsen, H. J. C. GROMACS: Fast, Flexible, and Free. *J. Comput. Chem.* **2005**, *26* (16), 1701−1718.
(96) Michaud-Agrawal, N.; Denning, E. J.; Woolf, T. B.; Beckstein, O. MDAnalysis: A Toolkit for the Analysis of Molecular Dynamics Simulations. *J. Comput. Chem.* **2011**, *32* (10), 2319−2327.
(97) Gowers, R.; Linke, M.; Barnoud, J.; Reddy, T.; Melo, M.; Seyler, S.; Domański, J.; Dotson, D.; Buchoux, S.; Kenney, I.; Beckstein, O. MDAnalysis: A Python Package for the Rapid Analysis of Molecular Dynamics Simulations. In *SCIPY Proceedings*, Austin, Texas, 2016; pp 98−105; DOI: 10.25080/Majora-629e541a-00e.

https://doi.org/10.1021/jacs.4c11226
J. Am. Chem. Soc. 2024, 146, 33616−33625